Available online at www.sciencedirect.com
SCIENCE DIRECT®
Advances in Space Research 37 (2006) 2269–2277
ADVANCES IN SPACE RESEARCH (a COSPAR publication)
www.elsevier.com/locate/asr

Remote sounding of atmospheric gravity waves with satellite limb and nadir techniques

Dong L. Wu [a,*], Peter Preusse [b], Stephen D. Eckermann [c], Jonathan H. Jiang [a], Manuel de la Torre Juarez [a], Lawrence Coy [c], Ding Y. Wang [d]

[a] Jet Propulsion Laboratory, MS 183-701, California Institute of Technology, Pasadena, California 91109, USA
[b] Institute for Chemistry and Dynamics of the Geosphere I, Forschungszentrum Jülich, Germany
[c] E.O. Hulburt Center for Space Research, Naval Research Laboratory, Washington, DC, USA
[d] Institut fur Meteorologie und Klimaforschung, Karlsruhe, Germany

Received 24 September 2004; received in revised form 5 July 2005; accepted 6 July 2005

Abstract

Recent advances in satellite techniques hold great potential for mapping global gravity wave (GW) processes at various altitudes. Poor understanding of small-scale GWs has been a major limitation to numerical climate and weather models for making reliable forecasts. Observations of short-scale features have important implication for validating and improving future high-resolution numerical models. This paper summarizes recent GW observations and sensitivities from several satellite instruments, including MLS, AMSU-A, AIRS, GPS, and CLAES. It is shown in an example that mountain waves with horizontal wavelengths as short as ~30 km now can be observed by AIRS, reflecting the superior horizontal resolution in these modern satellite instruments. Our studies show that MLS, AMSU-A and AIRS observations reveal similar GW characteristics, with the observed variances correlated well with background winds. As a complementary technique, limb sounding instruments like CRISTA, CLAES, and GPS can detect GWs with better vertical but poorer horizontal resolutions. To resolve different parts of the broad GW spectrum, both satellite limb and nadir observing techniques are needed, and a better understanding of GW complexities requires joint analyses of these data and dedicated high-resolution model simulations.

Keywords: Gravity waves; Satellite observations; Instrument filter; Wave sources

1. Introduction

Atmospheric gravity waves (GWs) have profound impacts on the Earth's weather and climate systems. Waves generated by flow over mountains, convection and jet-stream instability cause vertical advection that can produce organized cloud/precipitation bands (via adiabatic cooling) and net downstream effects on aerosol microphysics and trace constituent chemistry. These waves can also break, causing severe downslope windstorms and rotors near the surface, with significant vertical mixing in the upper troposphere and lower stratosphere (UTLS) and in the mesosphere and lower thermosphere (MLT). The momentum deposition from GW breaking at various altitudes yields body forces exerted on the synoptic circulation in the lower and upper atmosphere. These GW-induced body forces (so-called "GW drag"), either accelerative or decelerative, need to be taken into account by the coarse-resolution general circulation models (GCMs) that cannot resolve them. However, realistic representation or parameterization of GW drag is limited by lacks of observational guidance on global

* Corresponding author. Tel.: +1 818 393 1954; fax: +1 818 393 5065.
E-mail address: dwu@mls.jpl.nasa.gov (D.L. Wu).

0273-1177/$30
doi:10.1016/j.asr.2005.07.031

Nomenclature

AMSU-A	Advanced Microwave Sounding Unit-A
CHAMP	CHAllenging Minisatellite Payload
CIRA'89	COSPAR International Reference Atmosphere 1989
CLAES	Cryogenic Limb Array Etalon Spectrometer
CRISTA	Cryogenic Infrared Spectrometers and Telescopes for the Atmosphere
DoD	Department of Defense
ECMWF	European Center for Medium Range Weather Forecasts
EOS	Earth Observing System
FOV	Field Of View
GPS	Global Position System
HALOE	Halogen Occultation Experiment
HIRDLS	High Resolution Dynamics Limb Sounder
IFS	Integrated Forecasting System
ISAMS	Improved Stratospheric and Mesospheric Sounder
LEO	Low Earth Orbiter
LIMS	Limb Infrared Monitor of the Stratosphere
LOS	Line of Sight
MLS	Microwave Limb Sounder
MSX	Midcourse Space Experiment
NASA	National Aeronautics and Space Admin.
NOAA	National Oceanic and Atmospheric Admin.
NOGAPS	ALPHANavy Operational Global Atmospheric Prediction System with Advanced-Level Physics and High Altitude
SABER	Sounding of the Atmosphere using Broadband Emission Radiometry
SSMIS	Special Sensor MicrowaveImager/Sounder
TES	Tropospheric Emission Spectrometer
UARS	Upper Atmosphere Research Satellite
UKMO	United Kingdom Met Office

distributions of wave sources, propagation properties and overall momentum flux densities (e.g., Fritts and Alexander, 2003).

Recent advances in satellite remote sensing technology have begun to provide valuable information on these small-scale GWs and their global properties throughout the atmosphere. Satellite data acquired using limb and nadir techniques have demonstrated great potential for studying GW sources and propagation properties (e.g., Fetzer and Gille, 1994; Wu and Waters, 1996; Dewan et al., 1998; Eckermann and Preusse, 1999; Tsuda et al., 2000; Wu, 2004). This paper gives an overview of the relative advantages and disadvantages of various satellite techniques in terms of sensitivity to the GW spectrum. Recent progress in GW studies with MLS, AMSU-A, AIRS, GPS/CHAMP, and CLAES data are discussed, along with needs for a suite of complementary satellite sensors. A list of acronyms for satellite instruments and technological terms is provided at the end of this paper.

2. Satellite instrument viewing geometry

Satellite GW observations can be divided into three nominal groups, based on their viewing geometry in orbit (Fig. 1). "Category (a)" instruments adopt nadir/slant viewing and normally have small footprints and wide horizontal coverage. Since the vertical width of the temperature weighting function in this case is broad (>10 km), such instruments are sensitive to GWs with relatively large ratios of vertical-to-horizontal wavelengths (λ_z/λ_h). In other words, these instruments are sensitive to waves with high intrinsic frequencies since the hydrostatic irrotational GW dispersion relation is

$$\left|\frac{\lambda_z}{\lambda_h}\right| = \left|\frac{\omega}{N}\right|, \tag{1}$$

where ω is the wave's intrinsic frequency and N is buoyancy (Brunt-Väisälä) frequency. Instruments like this include AMSU-A, MSX, AIRS, TES (nadir), and SSMIS.

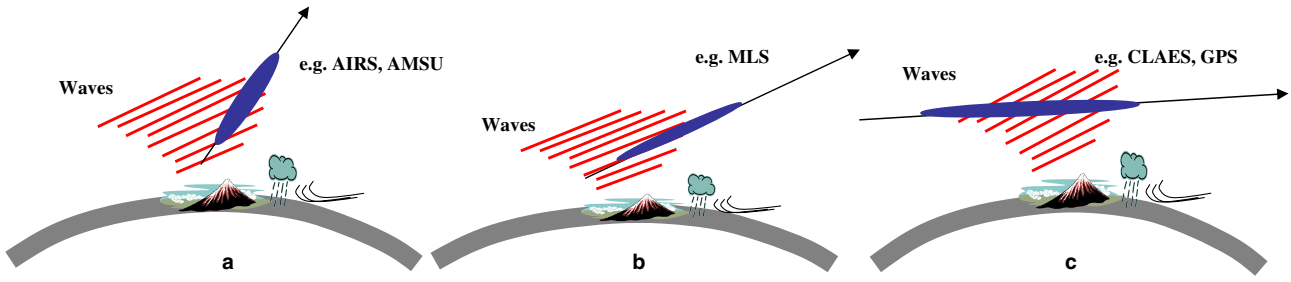

Fig. 1. Three types of satellite viewing geometry where GW-induced temperature perturbations can be measured: (a) nadir/slant path; (b) opaque limb path; (c) transparent limb path. Each has different sensitivities in horizontal and vertical wavelengths.

"Category (b)" instruments are somewhat similar to Category (a) instruments except operated at larger off-nadir slant viewing angles. These instruments normally have a narrow beamwidth and remain sensitive to waves whose phase fronts are roughly in parallel to the instrument LOS. MLS is an instrument of this kind, scanning at off-nadir angles of ~66°.

"Category (c)" instruments observe the atmosphere through a long transparent LOS path centered at the tangent point where most of the radiance signal comes from. Since such instruments normally have a narrow field of view (FOV), their vertical resolution is often excellent, while their horizontal resolution is coarse due to LOS-smearing. Thus, they are mostly sensitive to GWs with relatively small λ_z/λ_h ratios. Instruments in this group include LIMS, CLAES, ISAMS, CRISTA, SABER, HIRDLS, and GPS-LEO occultation.

3. Radiance/temperature perturbations and sensitivities to GWs

3.1. AMSU-A and AIRS radiances

AMSU-A 60-GHz radiances acquired with the downward-viewing strategy are sensitive to temperature perturbations of horizontal wavelengths >100 km and vertical wavelengths >10 km (Wu, 2004). The instrument adopts the cross-track scan up to ~±48° off the nadir. This sensor has been flown on three NOAA satellites (since 1998) and on NASA Aqua (since 2002). Although AMSU-A radiances are now operationally assimilated by some weather forecasting centers, GW information may not be fully preserved since data thinning and selecting procedures are typically needed (see, e.g., Baker and Campbell, 2004).

Fig. 2(a) shows an example where stratospheric mountain waves over southern Scandinavia were observed in the AMSU-A radiances at various altitudes. A unique feature of this downward viewing geometry is that it allows the waves' horizontal wavelengths to be explicitly resolved, unlike Category (c) limb viewers, for example, which horizontal wavelengths must be inferred indirectly (e.g., Preusse et al., 2002). The wave phase fronts at ~30–80 hPa (lower stratosphere) are aligned roughly north-south, showing the wave horizontal wavevector aligned approximately east-west, and the dominant horizontal wavelength is ~300 km. This is consistent with a long wavelength mountain wave forced by eastward flow across the southern Norwegian Mountains: a very similar event was observed and modeled on March 2, 2000 by Hertzog et al. (2002). This is buttressed by +12 h hindcasts using NRL's NOGAPS-ALPHA (T239L54 model: ~0.5° horizontal resolution), a high-altitude next generation version of NOGAPS for the US Navy's operational global numerical weather

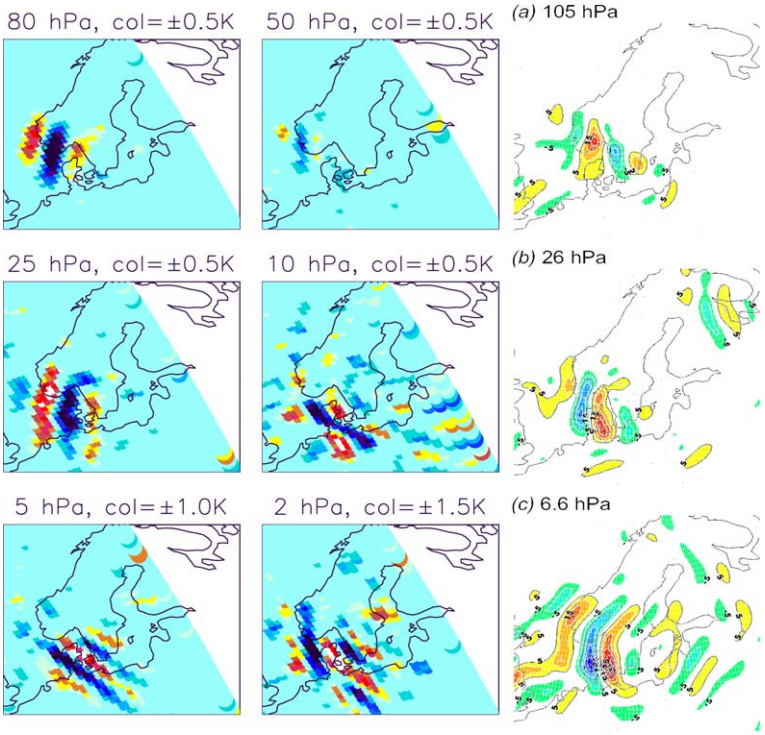

Fig. 2. A mountain wave event over Scandinavia on 14 January 2003 as (left) observed by NOAA-16 AMSU-A radiances at 1220 Z for several pressures (color range indicated at the top of each plot), and (right) seen in +12 h NOGAPS-ALPHA hindcast divergences (contours in units of 10^{-5} s^{-1}) valid for 14 January at 12 Z.

prediction (Eckermann et al., 2004). Fig. 2(b) shows plots of forecast divergence fields at various stratospheric pressure levels, where the nondivergent synoptic flow is removed to highlight divergence perturbations due to explicitly resolved GWs. Striking similarities are found in the geographical location and wavelengths of observed and modeled GWs in Fig. 2, despite some differences. This example demonstrates the great potential value of satellite observations such as these for validating high-resolution forecast products from state-of-the-art numerical weather prediction.

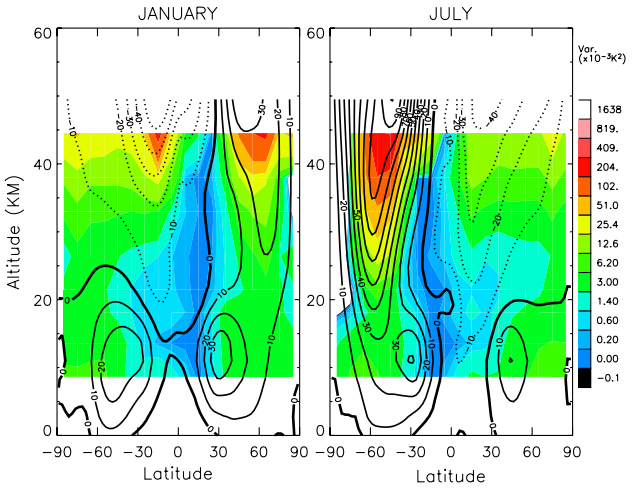

Fig. 3. NOAA-15 AMSU-A zonal-mean GW variances for January and July in 1998–2004. AMSU-A variances reveal a strong correlation with the wind speed where the zero wind speed corresponds to the lowest variances near the equator for both monthly climatologies. This wind-related property also exhibits in MLS GW variances (Fig. 7).

Good correlation is found between zonal mean AMSU-A GW variances (i.e., radiance perturbations from the nearest 5 measurements) in 1998–2004 and UKMO mean zonal winds (Fig. 3). The weak variances always occur near the zero wind regions and the largest variance is found in the core of the stratopause jets. The variances at winter high latitudes are greater in the Southern Hemisphere than in the Northern due to the stronger winter stratopause jet in the south. The similar wind-dependent variance difference is evident in the subtropics where the January variance at 15°S is noticeably stronger than the July variance at 15°N. Fig. 4 shows the GW variance map averaged from all AMSU-A viewing conditions at 5 hPa for June–August 2003, where the localized wave activity with quite small horizontal scales can be isolated. We infer this because variance enhancements are observed over very small sub-Antarctic islands, which are most likely associated with small horizontal wavelength mountain waves forced by flow across the islands.

The AMSU-A sensitivity to small-scale orographic waves requires further investigation, and may be aided

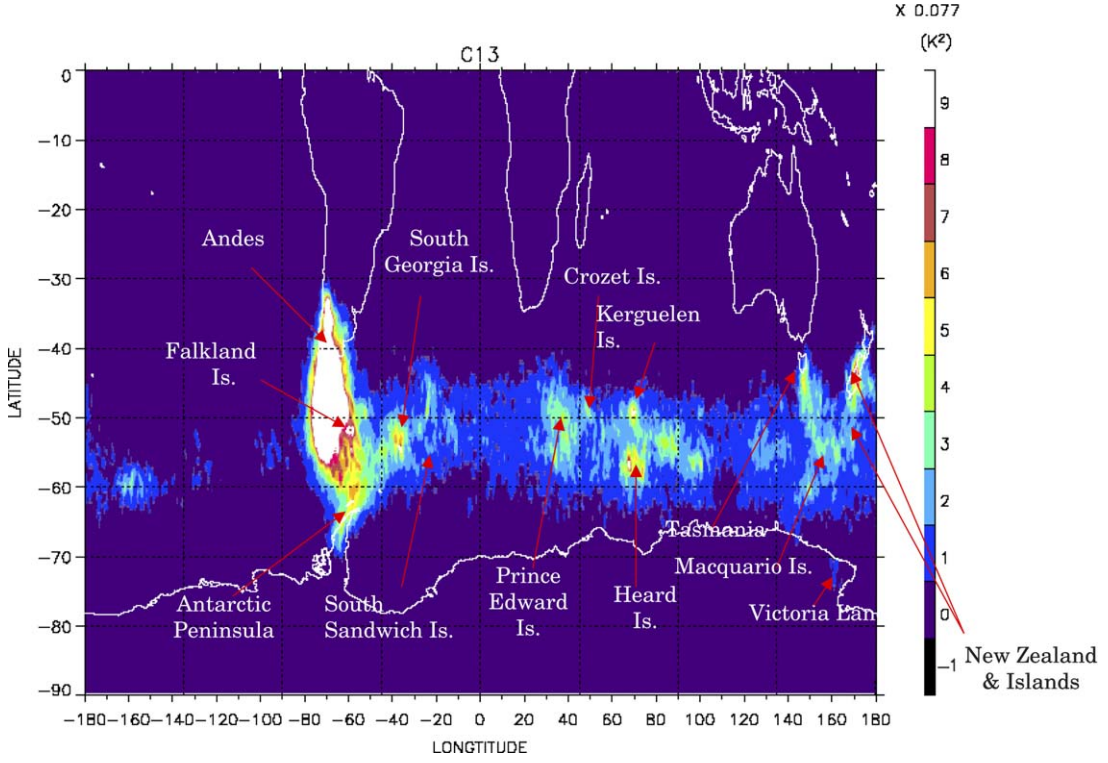

Fig. 4. A seasonal (June–August 2003) map of AMSU-A GW variances in the Southern Hemisphere (SH). The most prominent features in this 5-hPa map are the wave activities associated with the southern Andes and the Antarctic Peninsula. The 50-km AMSU-A horizontal resolution allows detection of GW-scale perturbations in a small region, which helps isolate wave features associated with sub-Antarctic islands. Coupled to jet-front generated wave components, these orographic sources can effectively enhance nearby wave activity in SH winters.

by observations from other high-resolution Category (a) satellites, such as AIRS. At nadir, AIRS has better horizontal resolution (15 km) but slightly poorer vertical resolution (~15 km) than AMSU-A. AIRS radiances can be spectrally averaged (for channels with the similar vertical weighting function) to reduce measurement noise. The averaged AIRS radiances allow to detect weaker GW perturbations that are barely detectable by AMSU-A on a daily basis. As shown in Fig. 5(a), the mountain waves observed by AMSU-A on 14 January 2003 (Fig. 2(a)) show up with much greater horizontal resolution in the AIRS radiances. The wave event over southern Scandinavia appears to be very transient, since the ascending (1100 Z) and descending (0100 Z) observations on 14 January are separated by only ~10 h, and became mostly absent in the map at 2000 Z on 15 January (not shown). Fig. 5(b) is another high-resolution AIRS map of mountain waves over southern South America, again consistent with variance enhancements noted for AMSU-A observations in Fig. 4.

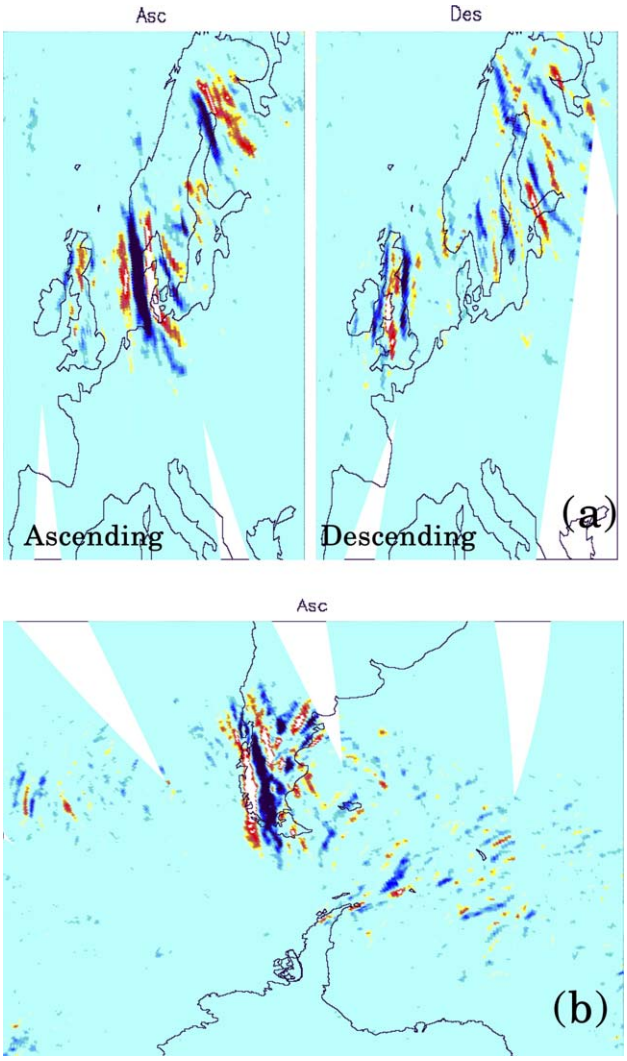

Fig. 5. (a) The same GW event over Scandinavia on 14 January 2003 as in Fig. 2 but observed by AIRS at 2.5 hPa from ascending (left) and descending (right) orbits. (b) Mountain waves over the southern Andes observed by AIRS at 2.5 hPa on 1 August 2004. The color range is ±2 K between blue and red.

The averaged AIRS radiances can detect weak convectively generated GWs on a daily basis, which are hardly seen in AMSU-A monthly maps. As shown in Fig. 6, convectively generated GWs are clearly evident in the tropical and subtropical stratosphere, emanating from well-known deep convection centers in South America and the Maritime Continent. Arc-like patterns at 2.5 hPa are common among the wave packets, suggesting that these waves are mostly propagating eastward, away from their point-like tropospheric sources of deep penetrative convection. These observations reveal that horizontal wavelengths typically range between 100 and 400 km, which are longer than the normal sizes of deep convective cells, suggesting the role of mesoscale coherent convective systems as an important source of stratospheric GWs. At 2.5 hPa the GW variance is noticeably weaker in the northern summer subtropics than in the southern one, consistent with the AMSU-A multi-year observations in Fig. 3.

3.2. MLS radiances

MLS limb radiances are sensitive to GW-induced temperature fluctuations with vertical wavelengths >10 km and horizontal wavelengths >30 km (e.g., Wu and Waters, 1996). The UARS MLS 63-GHz measurements from 1991 to 1997 produce global maps of GWs emanating from a variety of sources, including flow over mountains, convection, and jet-streams (McLandress et al., 2000; Jiang and Wu, 2001; Wu and Jiang, 2002; Jiang et al., 2004). The observed radiance variances are subject to the strong modulations by the background winds, which can be understood in terms of wave refraction by the flow (causing GW vertical wavelengths to change and become visible or invisible to the instrument) (Alexander, 1998). The observed and modeled GWs exhibit good agreement after the 3D instrument visibility function is taken into account (McLandress et al., 2000; Jiang et al., 2004).

Similar to Figs. 3 and 7 plots zonal mean GW variances but for the data of MLS ($z \sim 30$–80 km) and GPS/CHAMP ($z \sim 10$–27 km). As for AMSU-A, the zero wind speed contour correlates well with low MLS GW GW variances in the stratosphere but becomes less relevant for the lower-level GPS variances. The analysis of GPS/CHAMP data is deferred to the next section.

The new MLS instrument (118-GHz) on NASA's Aura satellite (launched in July 2004) continues to provide valuable GW observations. Aura MLS has similar horizontal resolution to UARS MLS but slightly better

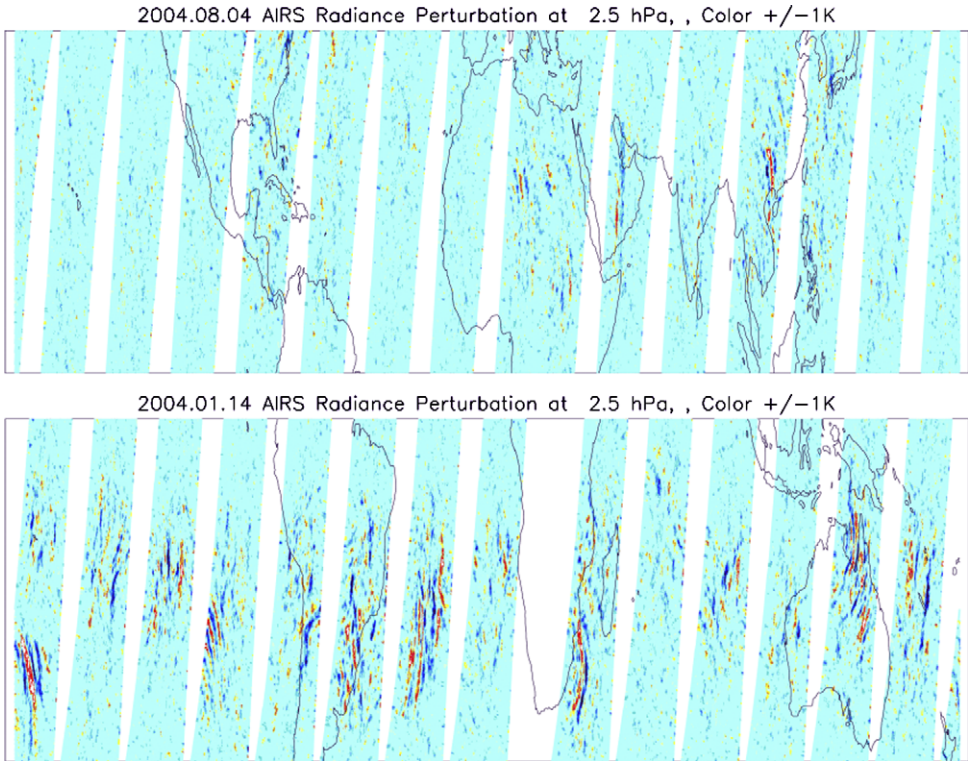

Fig. 6. AIRS 2.5-hPa radiance perturbation maps from descending orbits on 4 August 2004 (upper) and 14 January 2004 (lower). The color scales are ±1 K between blue and red.

(∼5 km) vertical resolution. Unlike UARS MLS, which viewed the atmospheric limb at 90° from the satellite motion, the scan plane of Aura MLS is parallel to the orbital plane, which yields the along-LOS resolution to ∼50–100 km depending on the incident angle. For long wavelengths, a truncation of ∼200 km is imposed as only a limited number of measurements can be used for the GW variance calculations. Fig. 8 shows zonal mean GW variances from MLS 118-GHz radiances on 3 August 2004, demonstrating a much improved signal-to-noise ratio over UARS MLS and a similar distribution to the monthly climatology in Fig. 7.

3.3. Temperatures from GPS occultation and CLAES

Temperature measurements from infrared (IR) limb sounding of optically thin emission lines and GPS occultation are two examples of transparent path limb sounding (TPLS), or Category (c) instruments. In the case of TPLS, the horizontal resolution is determined by the along-LOS resolution, which is typically ∼300 km long, if the instrument scans in the same plane of the satellite velocity. If the scan plane is 90° from the satellite velocity, on the other hand, the horizontal resolution is determined by the cross-LOS resolution. For GPS/CHAMP, the LOS/occultation plane can be as much as 70° from the satellite velocity, which means resolvable waves can have horizontal wavelengths <300 km since the instrument cross-LOS resolution is very narrow (∼3 km) (Lange and Jacobi, 2004). For UARS CLAES, the scan plane is 90° from the satellite velocity and the cross-LOS smearing is ∼50 km due to a 7 ∼ s integration time.

The sensitivity of TPLS instruments to GWs was first demonstrated for LIMS by Fetzer and Gille (1994) and for CRISTA by Fetzer and Gille (1994), which both acquired only a limited amount of data. Here we use CLAES measurements as our example of GWs resolved by IR TPLS. Fig. 9 plots zonal mean CLAES temperature variances for January and July 1992 CLAES observations, using the analysis method in Preusse et al. (2002), where background structures are removed using a wave 0–6 Kalman filter.

Temperature variances from GPS/CHAMP, shown earlier with MLS variances in Fig. 7, were restricted to vertical wavelengths <5 km to separate GW signals from planetary waves (PWs) and mean structures. A separation based on horizontal Kalman filtering could not be performed due to the sparser sampling of these occultation measurements (e.g., Tsuda et al., 2000). A feature in the GW variances inferred from these TPLS Category (c) measurements is that they have different zonal mean variance distributions. For example, both GPS (Fig. 7) and CLAES (Fig. 9) show a tropical maximum, which appears to result from low frequency long horizontal wavelength GWs that are supported in the tropics but

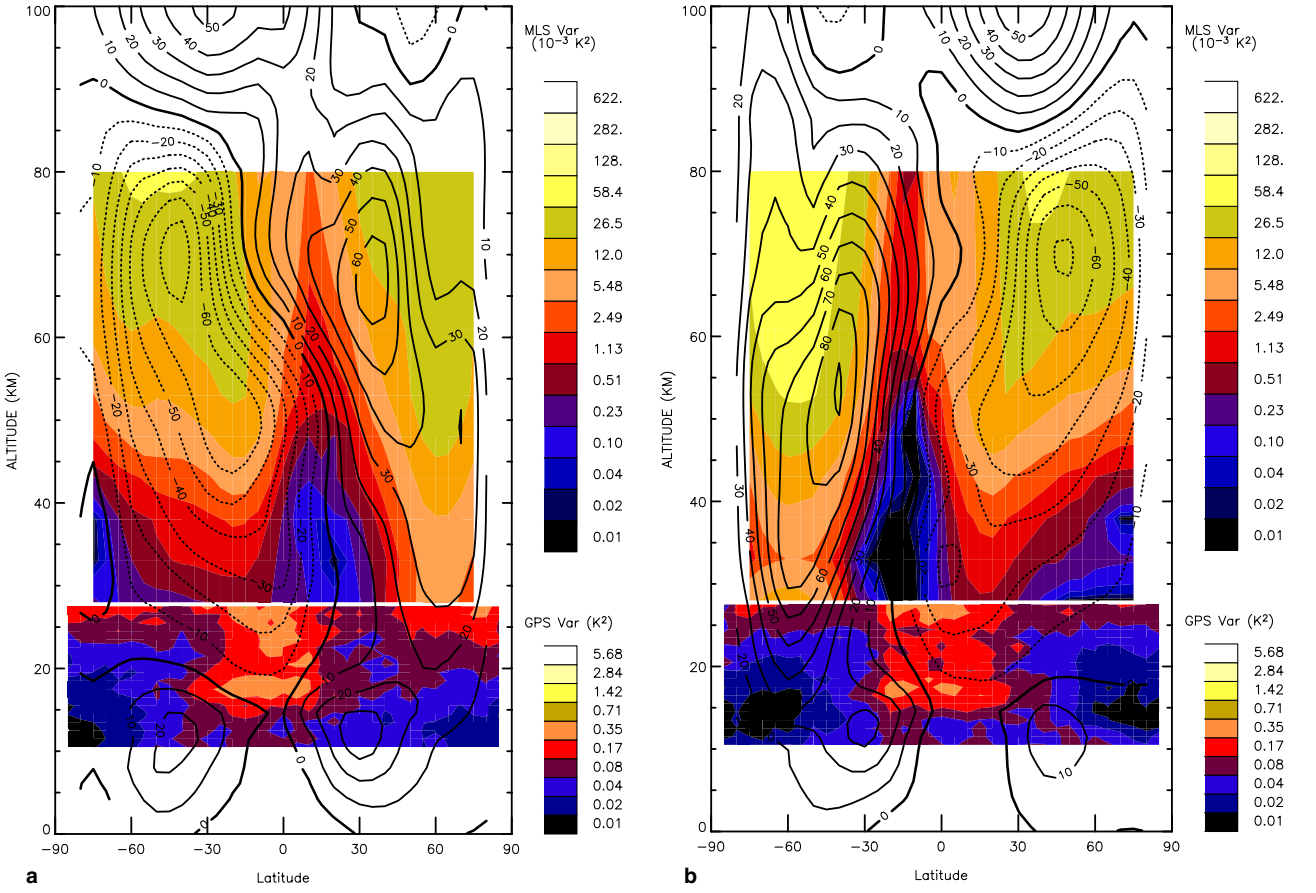

Fig. 7. MLS zonal mean GW variances (in colors) for (a) January and (b) July during 1991–1994 at 28–80 km altitudes and GPS/CHAMP GW variances for 2002–2003 at 10–25 km altitudes. The contours are CIRA 1986 zonal wind climatology. The 4-pt MLS limb scan data are used, which correspond to waves of short ($< \sim 60$ km) horizontal and long ($> \sim 10$ km) vertical wavelengths. The GPS variances are computed from the temperature profiles retrieved at JPL using the 42-km initialization. A 5-km vertical running window is applied to exclude large-scale wave components. A similar result was obtained by Ratnam et al. (2004).

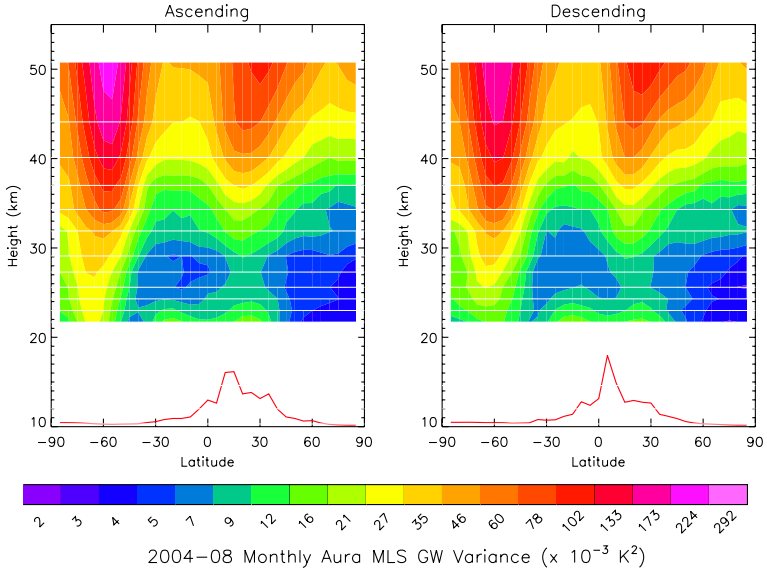

Fig. 8. Zonal mean GW variances from Aura MLS 118-GHz radiances for 3 August 2004. The instrument noise has been subtracted out from the radiance variance. The ascending and descending variances in this plot represent waves propagating southward and northward, respectively.

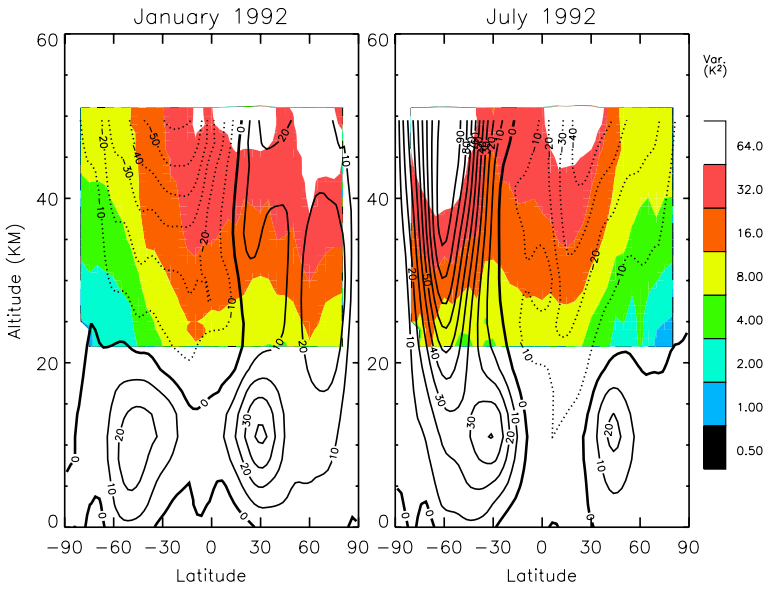

Fig. 9. CLAES zonal mean GW variances for January and July 1992, overlaid by the average UKMO zonal winds for the same period. CLAES temperature variances are much greater than GPS values at 25 km. Unlike MLS variances, CLAES data show weak sensitivity to the background wind speed.

cannot occur in the extratropics (Alexander et al., 2002; Ern et al., 2004). These waves are largely invisible to Category (a)–(b) instruments like AMSU-A and MLS since their vertical wavelengths are too short for these instruments to resolve. In summary, most of the differences in variance distributions between Category (a), (b) and (c) instruments can be related to their viewing geometry, and thus their different sensitivities to various portions of the GW spectrum. For example, Preusse et al. (2000) was able to re-produce MLS-like zonal mean variance in the stratosphere by reducing CRISTA vertical resolution to an "MLS-like" resolution.

4. Needs for synergetic satellite observations and future work

Simultaneous observations from multi-satellite sensors provide complementary views on various portions of the broad spectrum of atmospheric GWs. These wave variances vary substantially with time and location, much of which relates to the instrumental sensitivities to certain portions of the wave spectrum, and the wave refraction variation under changing background winds. What is clear is that no one class of instruments can provide all the information needed for a comprehensive understanding. Category (a), (b) and (c) instruments are all valuable in providing important measurements on different parts of the full GW spectrum.

Understanding complexities in global GW generation and propagation requires joint analyses of these satellite measurements and carefully targeted model simulations. Because waves can refract into and out of the visibilities of satellite sensors or numerical models, it remains challenging to assess the full nature of GW processes in the middle atmosphere. What are the variabilities of these distributions with respect to major wave sources, both geographically and temporally? How do we distinguish true GW interactions with background winds in dissipating variances from instrumental variance decreases as waves are refracted out of instrument visibility due

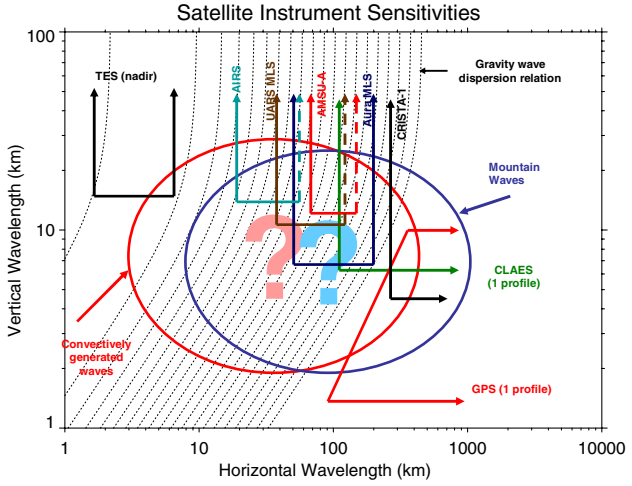

Fig. 10. Satellite instrument sensitivity limits in terms of cutoff GW vertical and horizontal wavelengths. The dashed lines denote the shortest truncation scale that can be achieved with nominal instrument operation. The lower horizontal wavelength cutoffs reflect the shortest of along-LOS and cross-LOS resolutions associated with sampling of each instrument, which depends on FOV smearing and sampling. The dotted lines represent the GW dispersion relation for each constant phase speed. The cycles with uncertainties denote GW power distributions hypothesized for convective and orographic sources.

to wind changes? (Alexander, 1998). These remain as tough questions for future research, but we believe current and future satellite measurements, taken in all, can lead to a better understanding of these complex issues. Fig. 10 summarizes the sensitivity limits of some recent satellite instruments in terms of λ_h and λ_z, overlaid next to GW wavelength ranges speculated for GWs from convective and orographic sources. This figure provides an initial depiction of such sensitivities, based on the instrument design, operation, and data analysis methods made available in literature or via private communications. More accurate characterization of these sensitivities is progressing and requires in-depth understanding of design and operation characteristics of each instrument. Furthermore, most instruments' horizontal sensitivities have a strong angular dependence that depends on the viewing angle and the satellite velocity vector (e.g., Jiang et al., 2004), so that in reality the instrument sensitivities in Fig. 10 are often 3D surfaces rather than 2D functions.

Acknowledgements

This work was performed at the Jet Propulsion Laboratory (JPL), California Institute of Technology, under a contract with the National Aeronautics and Space Administration (NASA), and funded through the JPL internal Research and Technology Development program. DLW and JHJ would like to acknowledge the support from NASA ACMAP program. SDE and LC acknowledge support for their work through the Office of Naval Research and NASA's Geospace Sciences Program. We thank the NOAA Satellite Active Archive center and the Near-line Archive Data Mining (NADM) in Goddard Earth Sciences Distributed Active Archive Center for making the AMSU and AIRS data available to this research.

References

Alexander, M.J. Interpretations of observed climatological patterns in stratospheric gravity wave variance. J. Geophys. Res. 103, 8627–8640, 1998.

Alexander, M.J., Tsuda, T., Vincent, R.A. On the latitudinal variations observed in gravity waves with short vertical wavelengths. J. Atmos. Sci. 59, 1394–1404, 2002.

Baker, N.L., Campbell, W.F. The impact of AMSU-A radiance assimilation in the US Navy's Operational Global Atmospheric Prediction System (NOGAPS), in: 13th Conference on Satellite Meteorology and Oceanography, 20–23 September to 17 June. American Meteorological Society, Norfolk, VA, p. 11, 2004, Paper P3.1, Preprint Vol.

Dewan, E.M., Picard, R.H., O'Neil, R.R., et al. MSX satellite observations of thunderstorm-generated gravity waves in mid-wave infrared images of the upper stratosphere. Geophys. Res. Lett. 25 (7), 939–942, 1998.

Eckermann, S.D., Preusse, P. Global measurements of stratospheric mountain waves from space. Science 286, 1534–1537, 1999.

Eckermann, S.D., McCormack, J.P., Coy, L., Allen, D., Hogan, T., Kim, Y.-J NOGAPS-ALPHA: A prototype high-altitude global NWP model, in: Symposium on the 50th Anniversary of Operational Numerical Weather Prediction, 14–17 June. American Meteorological Society, University of Maryland, College Park, MD, p. 23, 2004, Paper P2.6, Preprint Vol.

Ern, M., Preusse, P., Alexander, M.J., et al. Absolute values of gravity wave momentum flux derived from satellite data. J. Geophys. Res. 109 (D20), doi:10.1029/2004JD0004752, 2004.

Fetzer, E.J., Gille, J.C. Gravity wave variance in LIMS temperatures. Part I: variability and comparison with background winds. J. Atmos. Sci. 51, 2461–2483, 1994.

Fritts, D.C., Alexander, M.J. Gravity wave dynamics and effects in the middle atmosphere. Rev. Geophys. 41 (1), 1003, doi:10.1029/2001RG000106, 2003.

Hertzog, A., Vial, F., Dörnbrack, A., Eckermann, S.D., Knudsen, B.M., Pommereau, J.-P. In situ observations of gravity waves and comparisons with numerical simulations during the SOLVE/THESEO 2000 campaign. J. Geophys. Res. 107 (D20), 8292, doi:10.1029/2001JD001025, 2002.

Jiang, J.H., Wu, D.L. UARS MLS observations of gravity waves associated with the Arctic winter stratospheric vortex. Geophys. Res. Lett. 28, 527–530, 2001.

Jiang, J.H, Eckermann, S.D., Wu, D.L., Ma, J. A search for mountain waves in MLS stratospheric limb radiances from the winter Northern Hemisphere: data analysis and global mountain wave modeling. J. Geophys. Res. 109 (D3), D03107, doi:10.1029/2003JD003974, 2004.

Lange, M., Jacobi, C. Analysis of gravity waves from radio occultation measurements. Unpublished materials, 2004.

McLandress, C., Alexander, M.J., Wu, D.L. MLS observations of gravity waves in the stratosphere: a climatology and interpretation. J. Geophys. Res. 105, 11,947–11,967, 2000.

Preusse, P., Eckermann, S.D., Offermann, D. Comparison of global distributions of zonal-mean gravity wave variance inferred from different satellite instruments. Geophys. Res. Lett. 27, 3877–3880, 2000.

Preusse, P., Dornbrack, A., Eckermann, S.D., et al. Space-based measurements of stratospheric mountain waves by CRISTA-1. Sensitivity, analysis method, and a case study. J. Geophys. Res. 107 (D23), doi:10.1029/2001JD000699, 2002.

Ratnam, M.V., Tetzlaff, G., Jacobi, C. Global and seasonal variations of stratospheric gravity wave activity deduced from the CHAMP/GPS satellite. J. Atmos. Sci. 61, 1610–1620, 2004.

Tsuda, T., Nishida, M., Rocken, C., Ware, R.H. A global morphology of gravity wave activity in the stratosphere revealed by the GPS occultation data (GPS/MET). J. Geophys. Res. 105, 7257–7273, 2000.

Wu, D.L. Mesoscale gravity wave variances from AMSU-A radiances. Geophys. Res. Lett., L12114, doi:10.1029/2004GL019562, 2004.

Wu, D.L., Waters, J.W. Satellite observations of atmospheric variances: a possible indication of gravity waves. Geophys. Res. Lett 23, 3631–3634, 1996.

Wu, D.L., Jiang, J.H. MLS Observations of atmospheric gravity waves over Antarctica. J Geophys. Res. Atmos. 107 (D24), 4773, doi:10.1029/2002JD002390, 2002.